HHS Public Access

Author manuscript

Magn Reson Med. Author manuscript; available in PMC 2017 February 01.

Published in final edited form as:

Magn Reson Med. 2016 February ; 75(2): 845–851. doi:10.1002/mrm.25681.

Sensitivity of Chemical Shift-Encoded Fat Quantification to Calibration of Fat MR Spectrum

Xiaoke Wang[1,2], **Diego Hernando**[1], and **Scott B. Reeder**[1,2,3,4,5]

[1]Departments of Radiology, University of Wisconsin, Madison, WI

[2]Biomedical Engineering, University of Wisconsin, Madison, WI

[3]Medical Physics, University of Wisconsin, Madison, WI

[4]Medicine, University of Wisconsin, Madison, WI

[5]Emergency Medicine, University of Wisconsin, Madison, WI

Abstract

Purpose—To evaluate the impact of different fat spectral models on proton density fat-fraction (PDFF) quantification using chemical shift-encoded (CSE) MRI.

Material and Methods—Simulations and in vivo imaging were performed. In a simulation study, spectral models of fat were compared pairwise. Comparison of magnitude fitting and mixed fitting was performed over a range of echo times and fat fractions. In vivo acquisitions from 41 patients were reconstructed using 7 published spectral models of fat. T2-corrected STEAM-MRS was used as reference.

Results—Simulations demonstrate that imperfectly calibrated spectral models of fat result in biases that depend on echo times and fat fraction. Mixed fitting is more robust against this bias than magnitude fitting. Multi-peak spectral models showed much smaller differences among themselves than when compared to the single-peak spectral model. In vivo studies show all multi-peak models agree better (for mixed fitting, slope ranged from 0.967–1.045 using linear regression) with reference standard than the single-peak model (for mixed fitting, slope=0.76).

Conclusion—It is essential to use a multi-peak fat model for accurate quantification of fat with CSE-MRI. Further, fat quantification techniques using multi-peak fat models are comparable and no specific choice of spectral model is shown to be superior to the rest.

Keywords

fat quantification; spectral model of fat; proton density fat fraction; fat spectrum; non-alcoholic fatty liver disease; magnetic resonance imaging

Corresponding Author: Scott B. Reeder, M.D., Ph.D., Department of Radiology, 600 Highland Avenue, CSC E1/374, Madison, WI 53792-3252, 608-265-9964, sreeder@wisc.edu.

Introduction

Nonalcoholic fatty liver disease (NAFLD) is the most common chronic liver disease, affecting up to 30% of the adult U.S population (1). NAFLD is a risk factor for diabetes and cardiovascular disease, and can progress into cryptogenic cirrhosis and hepatocellular carcinoma (2,3). The diagnosis of NAFLD requires assessment of intracellular triglycerides in hepatocytes. Chemical shift-encoded (CSE) water fat imaging enables accurate quantification of proton density fat fraction (PDFF) over the entire liver. Compared with liver biopsy and single voxel MR spectroscopy (MRS) (4), CSE-MRI provides non-invasive spatially resolved quantification of liver fat. 3D coverage of the entire liver can be acquired within a single breath-hold (5–8). Extensive validation of confounder-corrected quantitative CSE-MRI have demonstrated equivalence of these methods to MRS (5–7,9–11)

In CSE-MRI, multiple images are acquired with increasing echo time (TE). A water image (W) and a fat image (F) are calculated by fitting the acquired data at each voxel to a signal model based on the chemical shift between fat and water (6,7). Fat fraction is then calculated as F/(W+F). To ensure that the calculation yields proton density fat-fraction (PDFF), a fundamental property of tissue that reflects the concentration of triglycerides (12), several confounding factors must be addressed. Such confounders include B_0 inhomogeneity (13), T1 bias (14,15), T2* signal decay (15–18), eddy currents (19,20), noise bias (14), and the spectral complexity of fat (18,21).

Compared with water, which has a single spectral peak, the complex structure of triglyceride molecules leads to complex and heterogeneous proton chemical shifts within the molecule. The different chemical shifts observed in a number of functional groups in fat molecules give rise to multiple peaks of fat signal in proton-based MRI. In early CSE-MRI techniques, a single-peak fat model (methylene peak) was generally assumed. However, this single-peak model accounts for only 70% of the total fat protons (22). A recent study showed that the single-peak model results in a biased estimate of PDFF that can be corrected by using a multi-peak spectral model of fat (21). In principle, the use of such a model requires independent estimation of the amplitude (and potentially other spectral parameters) of every fat peak. However, due to limited number of echo times typically acquired in CSE-MRI, it is not possible to individually resolve each fat peak. Consequently, CSE-MRI using a pre-calibrated multi-peak fat spectral model have been proposed (15,17,21), where the relative amplitudes and chemical shift of fat peaks are assumed to be known parameters. Therefore, compared with the single-peak model, no additional variables (degrees of freedom) are introduced into the estimation problem.

Pre-calibrated multi-peak models have been derived by MR spectroscopy or using dedicated CSE-MRI experiments with a large number of echo times (17,22,23). However, different models have been derived and applied in different studies. The various models differ in the number of peaks, chemical shift between peaks and relative amplitudes of the peaks. Although techniques using different spectral models have been validated for accurate fat quantification or water fat separation, there is no consensus as to which spectral model should be used.

The impact on PDFF estimation from the choice of spectral model of fat is unknown, and this lack of standardization has potential impact on the reproducibility of CSE-MRI for quantifying fat. The purpose of this study is to evaluate the sensitivity of PDFF mapping to the choice of multi-peak fat model by simulation and in vivo liver fat quantification.

Theory

In chemical shift-encoded (CSE) MRI, the acquired signal in a voxel in the presence of water and fat can be generally described as:

$$s_n = e^{i(\Delta\omega_0 \cdot TE_n)} \cdot \left(We^{i\phi_{0,w}} e^{-R2} w^* \cdot TE_n + FE^{i\phi_{0,f}} \cdot \sum_{p=1}^{P} \alpha_p e^{i2\pi \cdot f_p \cdot TE_n} e^{-R2_p^* \cdot TE_n}\right) \quad (1)$$

where s_n is the signal acquired at the n^{th} echo time TE_n, $\Delta\omega_0$, is the frequency offset due to local B_0 off-resonance $\varphi_{0,w}$, $\varphi_{0,f}$ are the initial phase of water and fat signal. The signal consists of one water peak and P fat peaks. W and F are the sum of all water signal and fat signal, respectively. The R2* decay rate of water is $R2_W^*$. The relative amplitude, relative frequency shift, and R2* decay rate of the p^{th} fat peak are denoted as a_p, f_p and $R2^*_p$, respectively. In general, $\varphi_{0,w}$, $\varphi_{0,f}$, $\Delta\omega_0$, $R2_W^*$, $a_1 \ldots a_P$, $f_1 \ldots f_P$, $R2^*_1 \ldots R2^*_p$ are the unknown parameters to be estimated.

In CSE-MRI, due to imaging time constraints, 6 echoes with maximum echo time of approximately 10–20ms (at 1.5T) are typically acquired, providing limited spectral resolution. To achieve robust water fat separation, the number of unknowns can be reduced by introducing assumptions to the general signal model in Eq (1). Two major and well-validated assumptions are commonly used 1) $R2^*$ of water and all fat peaks are all assumed to be equal (7,24), 2) the relative amplitude and chemical shift of all fat peaks are assumed to be known a priori based on other experimental data (17,21) (i.e. pre-calibrated fat spectrum). These assumptions lead to the following simplified signal model (18):

$$s_n = e^{i(\Delta\omega_0 \cdot TE_n)} \cdot \left(We^{i\phi_{0,w}} + Fe^{i\phi_{0,f}} \cdot \sum_{p=1}^{P} \alpha_p e^{i2\pi \cdot f_p \cdot TE_n}\right) e^{-R2^* \cdot TE_n} \quad (2)$$

where a_p, f_p are the known (ie: pre-calibrated) relative amplitude and frequency shift of the p^{th} fat peak. In a typical CSE-MRI acquisition, signals from multiple echoes acquired are fit, on a voxel-by-voxel basis, using the signal model in Eq (2) to estimate the six unknown parameters W, F, $\varphi_{0,w}$ and $\varphi_{0,f}$, $\Delta\omega_0$, and $R2^*$. A PDFF map then can be calculated using separated water and fat images, including correction for noise bias effects (14). This signal model has been successfully applied for PDFF quantification, and validated using MR spectroscopy-based fat quantification as a reference (6,7).

Further, eddy current effects can lead to undesired phase shifts between different echoes, introducing errors in CSE fat quantification. To address this challenge, fitting is often performed after taking magnitude of both sides of Eq (2), ie: “magnitude” fitting. When the phase in equation 2 is preserved, this is referred to as “complex” fitting. Magnitude fitting is relatively immune to eddy current related phase errors but suffers from reduced noise performance compared with complex fitting (25). Alternatively, a mixed fitting technique has been proposed where only the phase of the first echo is discarded in “single echo train”

acquisitions. Mixed fitting results in good robustness to phase errors relative to complex fitting, and improved noise performance relative to magnitude fitting (20).

The specific choice of pre-calibrated multi-peak fat model differs considerably between studies and there is no consensus as to which is the best and most appropriate spectrum to use. In recent works, Hamilton et al., measured the human liver fat spectrum as a 6-peak and a 9-peak model using spectroscopy on a 3T GE system (22). Ren et al., characterized the human subcutaneous and bone marrow fat spectrum using a 7-peak model, measured at 7T, using single-voxel stimulated echo acquisition mode STEAM spectroscopy (23). Wokke et al., derived 4- and 5-peak fat models by merging peaks that are close together in the 6-peak model(26). Yu et al., applied a self-calibrated fat quantification method which calibrated human liver fat spectrum on a 1.5T system as a 3 peak model (17).

The differences in number of peaks, frequency shifts relative to water, and relative amplitudes are summarized in Table 1. Among these fat models, 6,7 and 9-peak models are most commonly used in CSE fat quantification. The 9-peak model has been adopted by Berglund et al. (27), 6-peak model has been adopted by Hernando et al. (18), Hines et al. (7), Meisamy et al. (6). The 7-peak model has been used by Jonker et al. (28). An additional 3-peak model and 5-peak model have also been reported by Yokoo et al. (5,9).

Materials and Methods

Simulations

As part of a computer simulation, each spectral model of fat was compared with all other models in a pairwise manner. Specifically one model was used to generate a test signal (as the “true” fat model) at each TE, and the other spectral model (as the estimator fat model) was used to fit the test signals to estimate PDFF. All frequencies are based on 1.5T imaging. For each pair of spectral models of fat test signals were generated using the signal model in Eq (2) for simulated voxels with fat fractions ranging from 1% to 40%, and a fixed R2* of $40s^{-1}$ (typical for 1.5T liver imaging (29)). No noise were added. A combination of 6 echoes starting at 1.2ms, and spaced by 2.0ms were adopted. The initial phase of water and fat was assumed 0, and the initial field inhomogeneity was 2ppm. No eddy current induced phase was added to the first echo. Nevertheless, the phase of the first echo was discarded for both the magnitude and mixed fitting algorithms to better approximate the in vivo situation (20,25).

The PDFF was estimated by fitting the test signals to equation 2 using both magnitude and mixed fitting algorithms, using a different signal model as the estimator fat model. The estimated PDFF was then compared to the true PDFF using linear regression to determine the bias. This simulation was performed for all possible pairs of the fat models listed in Table 1.

Next, the effect of the choice of echo times on the PDFF bias caused by multi-peak model mismatch was also evaluated using simulations. Each combination contains 6 echoes with initial echo time (TE_{min}) and echo spacing (ΔTE) both ranging from 0ms to 3ms. For this simulation, the fat fraction was 30%, R2* = $40s^{-1}$, field strength 1.5T. Signal was generated

using the 6-peak model reported by Hamilton et al. as the “true” fat model and PDFF was estimated with 1, 3, 5, 7, 9-peak models. No noise was added to the test signals since we were evaluating the effects of bias in these simulations. Bias was calculated for each echo combination studied.

In vivo liver fat quantification

In vivo liver datasets from 41 patients were also analyzed. Data acquisition was performed on GE Signa HDxt 1.5T scanners, with either an 8-channel cardiac coil or an 8-channel torso coil. This dataset has been analyzed by previous studies (6,7) for different purposes, but reprocessed specifically and uniquely for this study.

CSE data were obtained using an investigational version of a multi-echo spoiled gradient echo (SGRE) sequence. All images were acquired in axial plane and obtained during a single 21s breath-hold, with the following imaging parameters: readout direction R/L, matrix size 256×128, 2D autocalibrated parallel imaging (30) with a nominal acceleration factor of 2 in both phase encoding directions, for an effective acceleration factor of 2.2 (due to central autocalibration lines), slice thickness 10mm, 24 slices, flip angle 5°, TR=13.7–14.9ms, BW= ±125kHz, mono-polar readout (flyback gradients), 6 echoes, TE_{min}=1.2ms,ΔTE=2.0ms. PDFF maps using the multi-echo SGRE data were reconstructed twice using each fat model listed in Table 1, once using magnitude fitting and once using mixed fitting algorithms, respectively for a total of 14 reconstructions for each dataset. Due to eddy current induced phase, pure complex fitting was not performed since phase shifts on the first echo caused by eddy currents were known to create bias. T1 bias was minimized by using a low flip angle and by performing a retrospective T1 correction for any residual T1 related bias (7) assuming a T1 of 568ms for water and 343ms for fat (31). Initial field maps were stabilized with a 3D graph cut algorithm (not publicly available through water-fat toolbox) (32). Mixed fitting and magnitude fitting were performed using Levenberg-Marquardt least-square fitting algorithm.

A single voxel STEAM-MRS spectrum was also acquired in a single breath-hold in every subject to provide a reference standard for fat fraction (33). MRS data were acquired in the right lobe of liver during a 21s breath-hold at 5 echo times (10, 20, 30, 40, 50 ms) enabling T2 correction. Typical voxel size was 20 × 20 × 25 mm^3, TR=3500ms, 2048 readout points, 1 average, and spectral width = ±2.5 kHz. MRS-PDFF was estimated from STEAM-MRS data. MRS data of individual coils were first combined using a singular-value decomposition (SVD) based method (34) implemented in Matlab (Mathworks, Natick, MA). In jMRUI (35), individual signal peak areas were estimated using the coil-combined data at each echo time with the AMARES (36) algorithm and prior knowledge as described by Hamilton et al. (22). Peak area estimates over all echo times were then fit into a mono-exponential curve for the estimation of peak-specific T2 and T2-corrected peak areas. Subsequently, total water and fat signals were calculated as the summation of their individual peak areas. MRS-PDFF was calculated as the ratio of T2 corrected total fat signal and the sum of T2-corrected water and fat signals (35,37).

For each patient, a region-of-interest (ROI) was co-localized with the STEAM voxel in the slice closest to the center of STEAM voxel. The PDFF was measured in a 20 × 20 mm^2

voxel and the two adjacent slices to match the STEAM voxel closely. MRI-based PDFF was then calculated by averaging the PDFF values within the three ROI's. This procedure was repeated for reconstructions using each spectral model of fat and fitting algorithms. The same ROI's were used for all reconstructions of the same patient to achieve perfectly co-registered MRI-PDFF values.

For each patient, STEAM PDFF were linearly regressed against 14 MRI-based PDFF values. 95% confidence intervals and p values were generated from applying a t-test to the estimate of slopes and intercepts to determine whether slopes are significantly different from 1 and intercepts are significantly different from 0 (ie: $p_{slope}<0.05$ or $p_{intercept}<0.05$).

Results

Simulations

In pairwise comparisons, for each pair of spectral models of fat, estimated PDFF was linearly regressed against true PDFF with excellent correlation ($r^2 > 0.998$) as expected. Thus, slopes close to 1 and intercepts close to 0 reflect equivalence between compared models. In Figure 1, A) C) show slopes, B) D) show intercepts in comparison of each pair of spectral models when magnitude fitting (A,B) and mixed fitting (C,D) were used as fitting algorithms. Each row shows the slope between a particular spectral model ("true" fat model) and every other model (estimator fat model) in each column. Between a single-peak model and any multi-peak model, greater errors were observed between estimated fat fraction and true fat fraction (slope< 0.79 or slope>1.22, |intercept| up to 1.20% for mixed fitting, slope<0.82 or slope>1.15, |intercept| up to 1.56% for magnitude fitting). Between any two multi-peak models, improved agreement was demonstrated: 0.94<slope<1.03, −0.51%<intercept<0.10% for mixed fitting, 0.89< slope<1.08, −0.39%<intercept<0.60% for magnitude fitting.

Figure 2 presents simulation results for the absolute bias in estimated PDFF over a range of initial echo times and echo spacings. Horizontal and vertical axes show echo spacing and initial echo times, respectively. The top row was reconstructed using mixed fitting and the bottom row was reconstructed using magnitude fitting. A clear dependence of bias on echo combination is seen for both fitting algorithms. For magnitude fitting, there is a range of echo combinations (near TE_{min}=1.25ms, ΔTE=2.3ms) that result in over 10% absolute bias regardless of the fat model used in estimation. For mixed fitting, the bias changes more gradually with echo times, and remains relatively low for lower initial echo times and echo spacings.

In vivo liver fat quantification

Figure 3 shows representative PDFF maps of a patient calculated using several spectral models of fat, for both mixed fitting and magnitude fitting algorithms. A clear PDFF offset can be observed between reconstructions using single-peak model and multi-peak models. Over all patients, linear regression showed strong correlation between STEAM PDFF and all MRI-based PDFF values (r^2>0.962). Further, slopes and intercepts of these regressions were calculated and are shown in Table 2, including the 95% confidence intervals and p values

generated from t-tests. Multi-peak models with both fitting algorithms exhibit better agreement with the MRS as reflected by the values of slopes and intercepts. Only 1-peak ($p_{slope}=3.76\cdot10^{-13}$ in magnitude fitting $p_{slope}=5.00\cdot10^{-16}$ in mixed fitting) model and 7-peak ($p_{slope}=4.42\cdot10^{-2}$) in magnitude fitting and mixed fitting) models were significantly different from the reference. Despite being significantly different from the reference, 7-peak model has much closer agreement with the reference than single–peak model (slope=1.05 compared with 0.76 for single-peak model).

Discussion

In this study we have analyzed the sensitivity of MRI-based CSE fat quantification to the choice of spectral model of fat, using both computer simulations and in vivo data acquired in patients. Spectral models of fat from previously published studies were used in this analysis and it was demonstrated that all multi-peak models showed greater accuracy for quantifying fat than the single-peak model. In addition, mixed fitting showed better agreement between the spectral models than magnitude fitting. Overall, these data demonstrate that multi-peak spectral modeling of fat is essential for accurate estimation of PDFF. However, no compelling evidence has been found to support any specific multi-peak spectral model of fat over the rest.

Among the discussed multi-peak spectral models of fat, the 7-peak model by Ren et al. was calibrated in subcutaneous fat while the others were all measured in liver. The results shown in this study indicate the 2 fat depots have similar fat spectral peaks. 3-peak (1.5T) and 7-peak (7T) models are also calibrated at different field strengths compared with other models (3T). The fact that these models are relatively interchangeable, suggests that MR spectroscopy is a reproducible tool for the measurement of fat spectrum in scanners at different field strength (1.5T – 7T).

In all signal estimation problems, bias will be introduced when there is discrepancy between the underlying physics (eg. true spectral model) and the signal model used in the estimation of the parameters of interest. In the case of PDFF estimation, the resulting bias will depend on factors such as the true PDFF and the choice of echo times and fitting method (eg: magnitude vs mixed fitting).

The choice of echo times is an important component of CSE-MRI based fat quantification. It has been shown that the choice of echo times has a large impact on the noise performance of the technique (13,38). Further, previous studies have shown that bias due to temperature-related effects (ie: model mismatch) is heavily influenced by the choice of echo times, and also the fitting method (39). In this study, we have shown that bias created by discrepancies in the true spectral model and the estimator model will depend on the choice of echo times. Interestingly, the bias increased markedly with longer echo spacing. Bias can be limited by shortening initial echo time and echo time spacing. It was also important to note that mixed fitting was more robust to changes in echo time (ie: had less bias) than magnitude based fitting, which is consistent with the study by Hernando et al. (39). This may explain the observation by Heba (40) that using a shorter echo train length may improve the accuracy of PDFF quantification using magnitude based fitting. A discrepancy between the underlying

physics and the spectral model used in CSE-MRI may explain why using fewer echoes appears to lead to less bias, as shown in that study.

This study has several limitations. Small differences between a spectral model of fat used for PDFF estimation and the actual spectra will reduce accuracy. However, we have demonstrated that the accuracy of PDFF quantification is relatively insensitive to different spectral models. Therefore, it is likely that errors introduced by small discrepancies in the spectral model relative to the true spectra are much smaller than the variability due to noise and other unrelated confounders. Large patient populations may be necessary to detect errors introduced by errors in the spectral model. Although, published data suggest relative uniformity in the triglyceride spectra across patients (22), variability in the spectra between patients could also introduce additional variability in the estimated PDFF. A second limitation is that all in vivo data and simulations were acquired at 1.5T. However, quantitative CSE-MRI is increasingly frequently performed on 3T scanners. The difference between these two platforms may result in different optimal echo times, which impacts the relative importance of the spectral models. In addition, this study did not consider the presence of liver iron overload. The high R2* introduced by the presence of iron may affect the relative impact of different fat models. Furthermore, all in vivo data were acquired at the same echo time not allowing further in vivo validation of the echo time dependence of fat signal model related bias. Overall, however, we believe that the conclusions drawn by this study will, in all likelihood, extend to 3T and when R2* is higher, although further work would be needed to confirm this speculation. Finally, this study is limited to “single R2*” signal models, where the R2* decay is assumed common for water and fat signals. Although dual R2* signal models have been proposed and studied in CSE-MRI, single R2* models have superior noise performance (18,24), have been shown to be accurate and robust (6,7), and the assumption that the R2* of water and fat peaks are very similar has been experimentally validated (24).

In conclusion, multi-peak spectral modeling of fat is essential for accurate estimation of tissue fat concentration, as measured by the proton density fat-fraction. Although spectral modeling is necessary, no specific choice of spectral model was shown to be superior, so long as one of the multi-peak models discussed in this work is used. Echo time combinations, such as shorter echo times, and the use of mixed fitting may be useful to minimize the impact of any model imperfections.

Acknowledgments

We acknowledge the use of the ISMRM Fat-Water Toolbox (http://ismrm.org/workshops/FatWater12/data.htm) for some of the reconstruction methods described in this article. We acknowledge the support of the NIH (R01 DK083380, R01 DK088925, K24 DK102595, and UL1TR00427). We also thank GE Healthcare for their support.

References

1. Szczepaniak LS, Nurenberg P, Leonard D, Browning JD, Reingold JS, Grundy S, Hobbs HH, Dobbins RL. Magnetic resonance spectroscopy to measure hepatic triglyceride content: prevalence of hepatic steatosis in the general population. Am J Physiol Endocrinol Metab. 2005; 288:E462–468. [PubMed: 15339742]

2. Smedile A, Bugianesi E. Steatosis and hepatocellular carcinoma risk. Eur Rev Med Pharmacol Sci. 2005; 9:291–293. [PubMed: 16231592]

3. Cuadrado A, Orive A, Garcia-Suarez C, Dominguez A, Fernandez-Escalante JC, Crespo J, Pons-Romero F. Non-alcoholic steatohepatitis (NASH) and hepatocellular carcinoma. Obes Surg. 2005; 15:442–446. [PubMed: 15826485]

4. Thomsen C, Becker U, Winkler K, Christoffersen P, Jensen M, Henriksen O. Quantification of liver fat using magnetic resonance spectroscopy. Magn Reson Imaging. 1994; 12:487–495. [PubMed: 8007779]

5. Yokoo T, Bydder M, Hamilton G, Middleton MS, Gamst AC, Wolfson T, Hassanein T, Patton HM, Lavine JE, Schwimmer JB, et al. Nonalcoholic fatty liver disease: diagnostic and fat-grading accuracy of low-flip-angle multiecho gradient-recalled-echo MR imaging at 1. 5 T. Radiology. 2009; 251:67–76. [PubMed: 19221054]

6. Meisamy S, Hines CD, Hamilton G, Sirlin CB, McKenzie CA, Yu H, Brittain JH, Reeder SB. Quantification of hepatic steatosis with T1-independent, T2-corrected MR imaging with spectral modeling of fat: blinded comparison with MR spectroscopy. Radiology. 2011; 258:767–775. [PubMed: 21248233]

7. Hines CD, Frydrychowicz A, Hamilton G, Tudorascu DL, Vigen KK, Yu H, McKenzie CA, Sirlin CB, Brittain JH, Reeder SB. T(1) independent, T(2) (*) corrected chemical shift based fat-water separation with multi-peak fat spectral modeling is an accurate and precise measure of hepatic steatosis. J Magn Reson Imaging. 2011; 33:873–881. [PubMed: 21448952]

8. Reeder SB, Sirlin CB. Quantification of liver fat with magnetic resonance imaging. Magn Reson Imaging Clin N Am. 2010; 18:337–357. ix. [PubMed: 21094444]

9. Yokoo T, Shiehmorteza M, Hamilton G, Wolfson T, Schroeder ME, Middleton MS, Bydder M, Gamst AC, Kono Y, Kuo A, et al. Estimation of hepatic proton-density fat fraction by using MR imaging at 3. 0 T. Radiology. 2011; 258:749–759. [PubMed: 21212366]

10. Zhong X, Nickel MD, Kannengiesser SA, Dale BM, Kiefer B, Bashir MR. Liver fat quantification using a multi-step adaptive fitting approach with multi-echo GRE imaging. Magn Reson Med. 2014; 72:1353–1365. [PubMed: 24323332]

11. Kuhn JP, Hernando D, Munoz del Rio A, Evert M, Kannengiesser S, Volzke H, Mensel B, Puls R, Hosten N, Reeder SB. Effect of multipeak spectral modeling of fat for liver iron and fat quantification: correlation of biopsy with MR imaging results. Radiology. 2012; 265:133–142. [PubMed: 22923718]

12. Reeder SB, Hu HH, Sirlin CB. Proton density fat-fraction: a standardized MR-based biomarker of tissue fat concentration. J Magn Reson Imaging. 2012; 36:1011–1014. [PubMed: 22777847]

13. Reeder SB, Pineda AR, Wen Z, Shimakawa A, Yu H, Brittain JH, Gold GE, Beaulieu CH, Pelc NJ. Iterative decomposition of water and fat with echo asymmetry and least-squares estimation (IDEAL): application with fast spin-echo imaging. Magn Reson Med. 2005; 54:636–644. [PubMed: 16092103]

14. Liu CY, McKenzie CA, Yu H, Brittain JH, Reeder SB. Fat quantification with IDEAL gradient echo imaging: correction of bias from T(1) and noise. Magn Reson Med. 2007; 58:354–364. [PubMed: 17654578]

15. Bydder M, Yokoo T, Hamilton G, Middleton MS, Chavez AD, Schwimmer JB, Lavine JE, Sirlin CB. Relaxation effects in the quantification of fat using gradient echo imaging. Magn Reson Imaging. 2008; 26:347–359. [PubMed: 18093781]

16. Reeder SB, Bice EK, Yu H, Hernando D, Pineda AR. On the performance of T2* correction methods for quantification of hepatic fat content. Magn Reson Med. 2012; 67:389–404. [PubMed: 21661045]

17. Yu H, Shimakawa A, McKenzie CA, Brodsky E, Brittain JH, Reeder SB. Multiecho water-fat separation and simultaneous R2* estimation with multifrequency fat spectrum modeling. Magn Reson Med. 2008; 60:1122–1134. [PubMed: 18956464]

18. Hernando D, Liang ZP, Kellman P. Chemical shift-based water/fat separation: a comparison of signal models. Magn Reson Med. 2010; 64:811–822. [PubMed: 20593375]

19. Yu, H.; Shimakawa, A.; Reeder, S.; McKenzie, C.; Brittain, J. Magnitude Fitting Following Phase Sensitive Water-Fat Separation to Remove Effects of Phase Errors. 2009 April; Proceedings 17th

Scientific Meeting, International Society for Magnetic Resonance in Medicine; Honolulu, USA. p. 461

20. Hernando D, Hines CD, Yu H, Reeder SB. Addressing phase errors in fat-water imaging using a mixed magnitude/complex fitting method. Magn Reson Med. 2012; 67:638–644. [PubMed: 21713978]
21. Reeder SB, Robson PM, Yu H, Shimakawa A, Hines CD, McKenzie CA, Brittain JH. Quantification of hepatic steatosis with MRI: the effects of accurate fat spectral modeling. J Magn Reson Imaging. 2009; 29:1332–1339. [PubMed: 19472390]
22. Hamilton G, Yokoo T, Bydder M, Cruite I, Schroeder ME, Sirlin CB, Middleton MS. In vivo characterization of the liver fat (1)H MR spectrum. NMR Biomed. 2011; 24:784–790. [PubMed: 21834002]
23. Ren J, Dimitrov I, Sherry AD, Malloy CR. Composition of adipose tissue and marrow fat in humans by 1H NMR at 7 Tesla. J Lipid Res. 2008; 49:2055–2062. [PubMed: 18509197]
24. Horng DE, Hernando D, Hines CD, Reeder SB. Comparison of R2* correction methods for accurate fat quantification in fatty liver. J Magn Reson Imaging. 2013; 37:414–422. [PubMed: 23165934]
25. Yu H, Shimakawa A, Hines CD, McKenzie CA, Hamilton G, Sirlin CB, Brittain JH, Reeder SB. Combination of complex-based and magnitude-based multiecho water-fat separation for accurate quantification of fat-fraction. Magn Reson Med. 2011; 66:199–206. [PubMed: 21695724]
26. Wokke BH, Bos C, Reijnierse M, van Rijswijk CS, Eggers H, Webb A, Verschuuren JJ, Kan HE. Comparison of dixon and T1-weighted MR methods to assess the degree of fat infiltration in duchenne muscular dystrophy patients. J Magn Reson Imaging. 2013; 38:619–624. [PubMed: 23292884]
27. Berglund J, Kullberg J. Three-dimensional water/fat separation and T2* estimation based on whole-image optimization--application in breathhold liver imaging at 1. 5 T. Magn Reson Med. 2012; 67:1684–1693. [PubMed: 22189760]
28. Jonker, JT.; Widya, RL.; Hammer, S.; Schinkel, LDv; Meer, RWvd; Koning, EJd; Bilo, HJ.; Webb, A.; Webb, HE.; Kan, HE., et al. 1.5T and 7T MR Spectroscopy of Tissue Specific Changes in Ectopic Fat Content in Response to Exercise Training in Type 2 Diabetes Mellitus Patients: The ATLAS-study. 2011 April; Proceedings 19th Scientific Meeting, International Society for Magnetic Resonance in Medicine; Melbourne, Australia. p. 872
29. Schwenzer NF, Machann J, Haap MM, Martirosian P, Schraml C, Liebig G, Stefan N, Haring HU, Claussen CD, Fritsche A, et al. T2* relaxometry in liver, pancreas, and spleen in a healthy cohort of one hundred twenty-nine subjects-correlation with age, gender, and serum ferritin. Invest Radiol. 2008; 43:854–860. [PubMed: 19002057]
30. Brau AC, Beatty PJ, Skare S, Bammer R. Comparison of reconstruction accuracy and efficiency among autocalibrating data-driven parallel imaging methods. Magn Reson Med. 2008; 59:382–395. [PubMed: 18228603]
31. de Bazelaire CM, Duhamel GD, Rofsky NM, Alsop DC. MR imaging relaxation times of abdominal and pelvic tissues measured in vivo at 3. 0 T: preliminary results. Radiology. 2004; 230:652–659. [PubMed: 14990831]
32. Hernando D, Kellman P, Haldar JP, Liang ZP. Robust water/fat separation in the presence of large field inhomogeneities using a graph cut algorithm. Magn Reson Med. 2010; 63:79–90. [PubMed: 19859956]
33. Cassidy FH, Yokoo T, Aganovic L, Hanna RF, Bydder M, Middleton MS, Hamilton G, Chavez AD, Schwimmer JB, Sirlin CB. Fatty liver disease: MR imaging techniques for the detection and quantification of liver steatosis. Radiographics. 2009; 29:231–260. [PubMed: 19168847]
34. Bydder M, Hamilton G, Yokoo T, Sirlin CB. Optimal phased-array combination for spectroscopy. Magn Reson Imaging. 2008; 26:847–850. [PubMed: 18486392]
35. Naressi A, Couturier C, Devos JM, Janssen M, Mangeat C, de Beer R, Graveron-Demilly D. Java-based graphical user interface for the MRUI quantitation package. MAGMA. 2001; 12:141–152. [PubMed: 11390270]

36. Vanhamme L, van den Boogaart A, Van Huffel S. Improved method for accurate and efficient quantification of MRS data with use of prior knowledge. J Magn Reson. 1997; 129:35–43. [PubMed: 9405214]

37. Sharma P, Martin DR, Pineda N, Xu Q, Vos M, Anania F, Hu X. Quantitative analysis of T2-correction in single-voxel magnetic resonance spectroscopy of hepatic lipid fraction. J Magn Reson Imaging. 2009; 29:629–635. [PubMed: 19243059]

38. Reeder SB, McKenzie CA, Pineda AR, Yu H, Shimakawa A, Brau AC, Hargreaves BA, Gold GE, Brittain JH. Water-fat separation with IDEAL gradient-echo imaging. J Magn Reson Imaging. 2007; 25:644–652. [PubMed: 17326087]

39. Hernando D, Sharma SD, Kramer H, Reeder SB. On the confounding effect of temperature on chemical shift-encoded fat quantification. Magn Reson Med. 2014; 72:464–470. [PubMed: 24123362]

40. Heba, ER.; Hamilton, G.; Sirlin, CB.; Wolfson, T.; Gamst, A.; Loomba, R.; Middleton, MS. Agreement of 2-, 3-, 4-, 5- and 6-echo MRI-PDFF with MRS-PDFF in 580 adults with known or suspected non-alcoholic fatty liver disease (NAFLD). 2014 April; Proceedings 22th Scientific Meeting, International Society for Magnetic Resonance in Medicine; Milan. p. 138

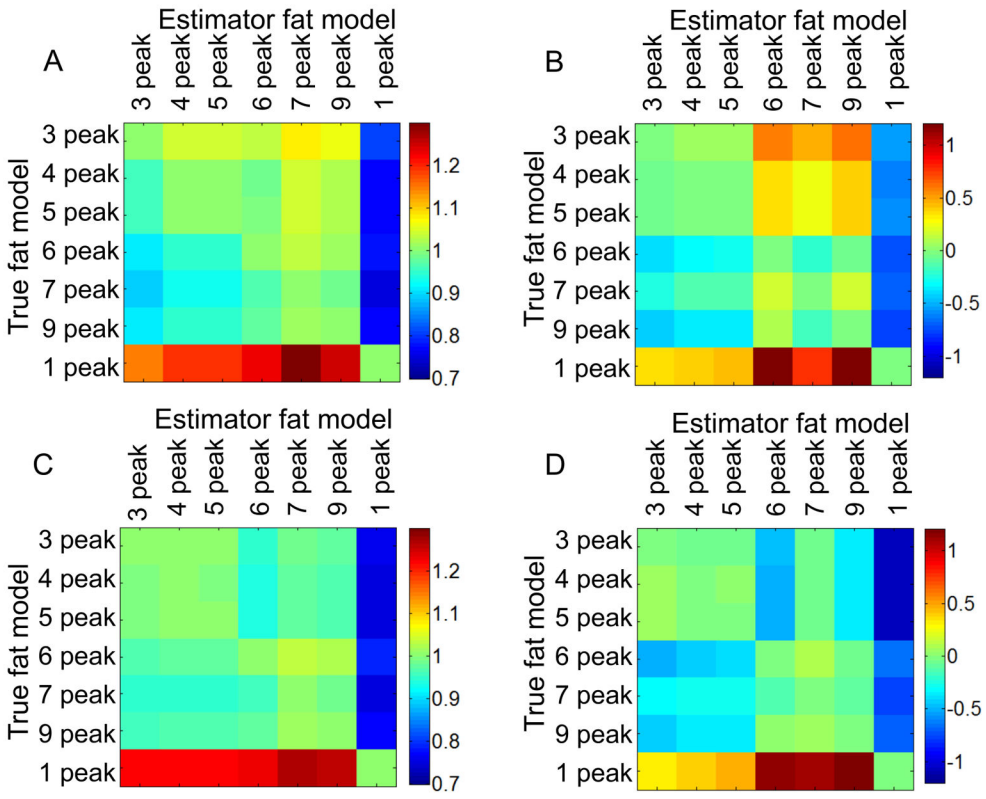

Figure 1.

Multi-peak models demonstrate better agreement with each other than with the single peak spectral model of fat. Results are from simulations comparing, in a pairwise manner, different spectral models of fat. The color coding plots the slope (A, C) and intercept (B, D) from linear regression of estimated PDFF with true fat fraction, for magnitude fitting (A,B) and mixed fitting (C, D).

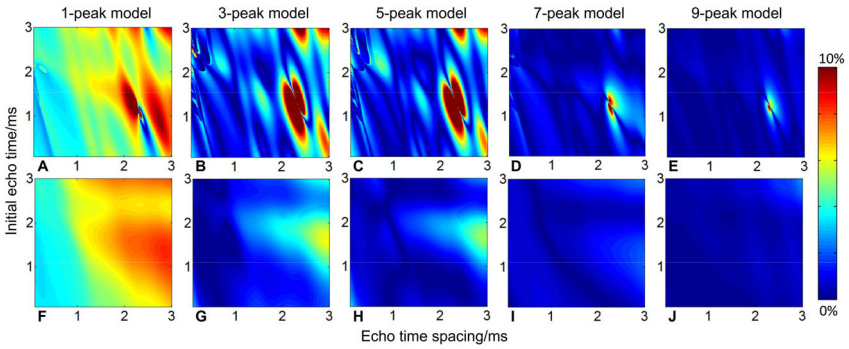

Figure 2.

In general, mixed fitting has lower bias than magnitude fitting and is less sensitive to the choice of spectral model of fat. Absolute biases from simulated PDFF estimate resulting from difference between “true” fat model (6-peak model) and estimator fat model (1-, 3-, 5-, 7-, 9-peak models) are presented for mixed fitting (A, B, C, D, E) and for magnitude fitting (F, G, H, I, J). The bias is shown to be a function of echo times. For certain echo time combinations, magnitude fitting can lead to large bias (>10%) even from small model differences, while mixed fitting had lower bias. particularly for 7-peak and 9-peak models

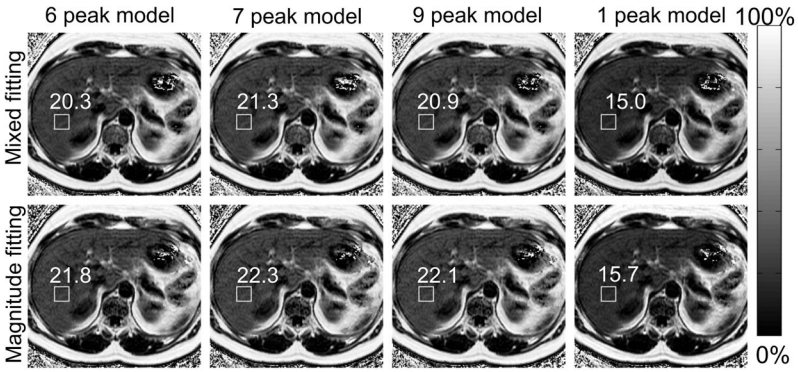

Figure 3.

Single-peak model produced substantially different liver fat fraction using 6-, 7-, and 9-peak spectral models of fat. PDFF maps from one patient reconstructed using mixed fitting (top row) and magnitude fitting (bottom row) for 4 different spectral models of fat. T2-corrected STEAM MRS-PDFF was 20.9% in this patient. The location of the steam voxel and Co-localized MRI-PDFF measurements are shown in the figure.

Table 1

List of different multi-peak spectral models of fat used in this work.

Peaks	Frequency relative to water (ppm)	Relative amplitude (%)	Reference
1	−3.4	100	n/a
3	0.73, −2.49, −3.29	8, 17, 75	Yu (17)
4	0.73, −2.49, −3.27, −3.68	8, 15, 72, 4	Wokke (26)
5	0.73, −2.35, −2.54, −3.27, −3.68	8, 5, 10, 72, 4	Wokke (26)
6	0.6, −0.5, −1.95, −2.6, −3.4, −3.8	4.7, 3.9, 0.6, 12, 70, 8.8	Hamilton (22) Hernando (18) Meisamy (6) Hines (7)
7	0.61, −1.93, −2.45, −2.67, −3.11, −3.4, −3.8	4.2, 1.5, 6.6, 9.6, 7.1, 62.7, 8.3	Ren (23), Jonker (28), Zhong (10)
9	0.59, 0.49, −0.5, −1.95, −2.46, −2.68, −3.1, −3.4, −3.8	3.7, 1, 3.9, 0.6, 5.8, 6.2, 5.8, 64.2, 8.8	Hamilton (22), Berglund (27)

Table 2

All multi-peak fat models agree closely with the reference standard (MRS-PDFF), as evidenced by regression results. Results of the linear correlation of MRI-PDFF and MRS-PDFF are tabulated for the 7 spectral models and the two fitting methods. Coefficient of determination, slope and intercept of the linear regression are all listed, including 95th percentile confidence intervals. Overall, multi-peak models including 7-peak model demonstrate better correlation and agreement with MRS than single-peak model as reflected by the values of slope and intercept estimate. No significant difference (p=0.05) was observed for multi-peak models expect 7-peak model using both fitting methods. Further, mixed fitting demonstrates slightly stronger correlation and agreement than does magnitude fitting, although the differences are small.

ββ	R^2	Slope [95th CI]	p-value (slope)	Intercept (%)[95th CI]	p-value (intercept)
Magnitude Fitting					
1-peak	0.974	0.770 [0.726, 0.814]	$3.755 \cdot 10^{-13}$	−0.406 [−0.891, 0.078]	0.098
3-peak	0.962	0.952 [0.900,1.004]	0.068	−0.284 [−0.852, 0.284]	0.318
4-peak	0.974	0.967 [0.916,1.019]	0.210	−0.295 [−0.868, 0.278]	0.304
5-peak	0.974	0.967 [0.916, 1.019]	0.214	−0.293 [−0.866, 0.279]	0.307
6-peak	0.978	1.035 [0.979, 1.091]	0.219	−0.282 [−0.907, 0.334]	0.357
7-peak	0.977	1.060 [0.988, 1.109]	0.041	−0.287 [−0.912, 0.349]	0.372
9-peak	0.970	1.050 [0.993, 1.107]	0.083	−0.287 [−0.914, 0.339]	0.360
Mixed Fitting					
1-peak	0.978	0.760 [0.723, 0.797]	$4.996 \cdot 10^{-15}$	−0.421 [−0.830,−0.012]	0.044
3-peak	0.979	0.967 [0.920,1.013]	0.151	−0.317 [−0.829, 0.194]	0.217
4-peak	0.979	0.975 [0.929,1.021]	0.281	−0.326 [−0.838, 0.185]	0.205
5-peak	0.979	0.975 [0.929,1.022]	0.292	−0.324 [−0.835, 0.188]	0.209
6-peak	0.982	1.008 [0.964, 1.053]	0.703	−0.373 [−0.864, 0.118]	0.133
7-peak	0.983	1.047 [1.001, 1.092]	0.044	−0.313 [−0.813 0.188]	0.214
9-peak	0.981	1.045 [0.997, 1.092]	0.063	−0.358 [−0.880 0.164]	0.174